

Effects of ZnO Sintering Additive on the Sintering Behavior and Conductivity of YSZ Solid Electrolyte

Fang Yang¹, Hao Fang¹, Qian Hu¹, Chunjun Zhao¹, Xiuzhen Qian¹, Chunhua Zhao^{1,*}

¹ Key Laboratory for Ultrafine Materials of Ministry of Education, School of Materials Science and Engineering, East China University of Science and Technology, Shanghai 200237, China

*E-mail: zhaochh@ecust.edu.cn

Received: 8 June 2017 / Accepted: 4 July 2017 / Published: 13 August 2017

The effects of ZnO sintering additive on the sintering behavior and electrochemical properties of YSZ-based solid electrolyte were investigated. With the addition of 3 mol% ZnO, the linear shrinkages of YSZ at 1200 °C increased from 7.1% to 15%, and the relative density at 1200°C increased from 82% to 94.6%. XRD confirmed that a small amount of Zn can be incorporated into the fluorite lattice, and EDX result showed that ZnO mainly distributed at the grain boundary. ZnO modified YSZ had denser structure and fewer pores than YSZ. The increased densification of YSZ by ZnO addition can significantly increase the grain and total conductivities. Compared with YSZ, the total conductivity of 2 mol% ZnO modified YSZ increased from 0.013 to 0.021 S·cm⁻¹ at 800 °C.

Keywords: ZnO modified YSZ; Sintering property; Electrochemical property; Solid oxide electrolyte

1. INTRODUCTION

Solid oxide fuel cell (SOFC) is an electrochemical device that can directly convert the electrochemical energy into electrical energy efficiently, which has attracted great attention of people [1, 2]. And solid oxide electrolyte, as the most important part of SOFC, has been thoroughly researched. Yttria stabilized zirconia (YSZ) has been widely used as an electrolyte in SOFC stacks due to its excellent stability and pure ionic conductivity in fuel and air atmosphere at typical operating temperatures [3]. Co-sintering of electrodes and electrolyte is the most cost-effective technology to prepare SOFC. However, the densification temperatures for commercial zirconia-based electrolyte are over 1300 °C [4]. When the sintering temperature is above 1250 °C, YSZ may react with the cathode and the performance of the SOFC will decrease. So, reducing the sintering temperature of YSZ was very important and a lot of research work about the sintering behavior of YSZ were done [5].

The sintering behavior can be improved by two ways: using nano-scaled powders and adding sintering additives. Relative density higher than 99% can be got at 1450 °C by using nano-sized YSZ powders prepared by polyethylene glycol (PEG) assisted coprecipitation coupling with azeotropic distillation drying process [6]. But nano-sized YSZ showed lower stability than micro-sized YSZ at high temperature [7]. At the same time, the fabrication of nano-sized powder requires a flexible process, which increases the cost and limits their commercial application. Adding appropriate sintering additives can decrease the sintering temperature of ceramics effectively. ZnO has been proven to be an ideal sintering additive [8-10]. The solution of ZnO in YSZ and the effects of ZnO on the sintering behavior and electrical properties were studied by some researchers.

But contradictory conclusions about the solubility of Zn in fluorite structure or Zn content on electrical properties were drawn in previous research work. Marcomini et al. showed that ZnO solubility in 8YSZ (8 mol% Ytria doped zirconia) is of the order of 3 mol% at the sintering temperature of 1300 °C [8]. Based on the Electron probe micro-analyzer (EPMA) and X-ray diffractometer (XRD) measurement of Y-TZP (Y₂O₃-doped tetragonal zirconia polycrystals)-*x* wt.%ZnO, NAKAYAMA et al. suggested that ZnO didn't dissolve into Y-TZP [9]. According to the XRD results, Liu et al. proved that ZnO and 8YSZ can form a solid solution when less than 10wt.% ZnO was added into 8YSZ [10]. Marcomini et al. suggested that the conductivity of 8YSZ at 350 °C decreased with the increase of ZnO when ZnO content is less than 20 vol.% [8]. By using impedance spectra, Liu et al. analyzed the effects of ZnO addition on grain and grain boundary conductivities at 300 °C. Overall, the grain conductivity decreased and the grain boundary conductivity increased with the addition of ZnO [10]. However, these authors didn't measure the electrical behaviors at higher temperature. At the same time, few YSZs can be sintered below 1300 °C.

In this work, the effect of ZnO addition on the sintering behavior of YSZ was studied. The structure, microstructure, and electrical properties of the ZnO-added samples sinter at 1200 °C were given.

2. EXPERIMENTAL

(Y₂O₃)_{0.08}(ZrO₂)_{0.92} (YSZ, 99.9% purity, Ningbo SOFCMAN Energy Technology Co., Ltd, China) with the average particle size of 0.5 μm and Zn(CH₃COO)₂·2H₂O (AR) (Sinopharm Chemical Reagent Co.,Ltd, China) were used as raw materials. Zn(CH₃COO)₂·2H₂O were thoroughly mixed with YSZ in an agate mortar. At high temperature Zn(CH₃COO)₂·2H₂O will be decomposed into ZnO. The samples without ZnO, and with *x* mol% ZnO (relative to 1mol YSZ) were labeled as YSZ and *x*ZYSZ. Then the precursors were calcined at 800 °C for 4 h. The calcined powders were milled in ethanol, dried, and blended with an organic binder. Disk-shaped powder compacts of diameter 5 mm were formed by uniaxial pressing at 200 MPa. The green disks were then sintered at 1150 and 1200 °C for 10 h in air and furnace-cooled to room temperature.

Phase composition was identified by using XRD with a Philips X-Pert diffractometer using the CuKα radiation (λ = 0.15418 nm) with a step size of 0.0167°. The densification behavior of the powders were studied with a dilatometer (Netzsch DIL 402C, Germany) in an air flow at a heating rate of

10 °C/min using a cylindrical powder compact of length 1.5 cm and diameter 0.5 cm. The density ρ was measured using Archimedes method. The relative density ρ_{rel} was determined according to the formula $\rho_{rel} = \rho / \rho_{th}$, where ρ_{th} is the theoretical density calculated from the lattice parameter as obtained from the XRD results. The microstructures of the sintered ceramics were observed by scanning electron microscope (SEM, Hitachi X-600, Japan); prior to the examination, samples were polished, and thermally etched at 1150 °C in air for 30 min. Zn distribution was measured by SEM (Hitachi S-4800, Japan) coupled with INCA energy-dispersive X-ray spectroscopy (EDX). For measuring the electrical conductivity, the two opposite sides of the sintered disks were polished and coated with silver paste, heated at 600 °C for metallization and quenched to room temperature. Gold wires were attached as electrode leads. Three samples for each component were used to measure the conductivities. For the AC impedance measurement, we used an AC impedance analyzer (Chenhua CHI604E, China) over the frequency range of 1 Hz to 105 Hz. All the impedance diagrams were normalized by the pellet geometrical factor.

3. RESULTS AND DISCUSSION

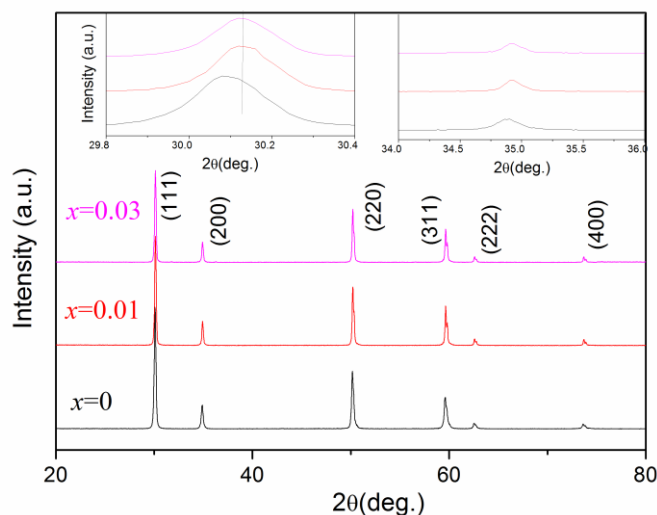


Figure 1. The X-ray patterns of YSZ, 1ZYSZ and 3ZYSZ sintered at 1200 °C.

The XRD patterns show that YSZ, 1ZYSZ and 3ZYSZ possess a single-phase cubic fluorite structure and no secondary phase was observed (Fig. 1) [11]. The diffraction peaks of the (111) plane were enlarged, as shown in the insert graph of Fig. 1. Compared with pure YSZ, the peak position of ZnO modified YSZ shifts to the right which can be attributed to the dissolution of ZnO into the fluorite lattice. The peaks of 1ZYSZ and 3ZYSZ keep at almost the same position, which means that less than 1 mol% ZnO can be doped into the fluorite lattice. But from Fig. 1, no ZnO phase was observed. Two possibilities can be used to explain the result: the low content of ZnO which cannot be detected by XRD or ZnO existed as an amorphous state. The lattice parameters (a) of YSZ and ZnO modified YSZ

are 5.1402 and 5.1361 Å, respectively. When ZnO is dissolved in the lattice, the reaction (using Kroeger-Vink notation) can be expressed as: $\text{ZnO} \rightarrow \text{Zn}_{\text{Zr}}^{\text{n}} + \text{V}_{\text{O}}^{\text{..}} + \text{O}_{\text{O}}^{\text{x}}$. The effective ionic coordination number (8) radius for Zn^{2+} , Y^{3+} , and Zr^{4+} are 90, 101.9, and 84 pm, respectively [12]. The substitute of Zr^{4+} by Zn^{2+} should cause the increase of a because Zn^{2+} has a larger ionic radius than Zr^{4+} . Here, the decrease of a by Zn doping can be attributed to the production of oxygen vacancy.

The densification behavior of the green compacts of YSZ and 3ZYSZ were performed in an air flow at a heating rate of $10^{\circ}\text{C min}^{-1}$, as shown in Fig. 2. It can be seen that ZnO added YSZ has higher shrinkage rate than YSZ. With 3 mol% ZnO addition, the maximum shrinkage temperature decreased by 50°C , and the linear shrinkages at 1200°C increased from 7.1% to 15%. Clearly, 3 mol% ZnO addition can effectively improve the sintering activity of YSZ.

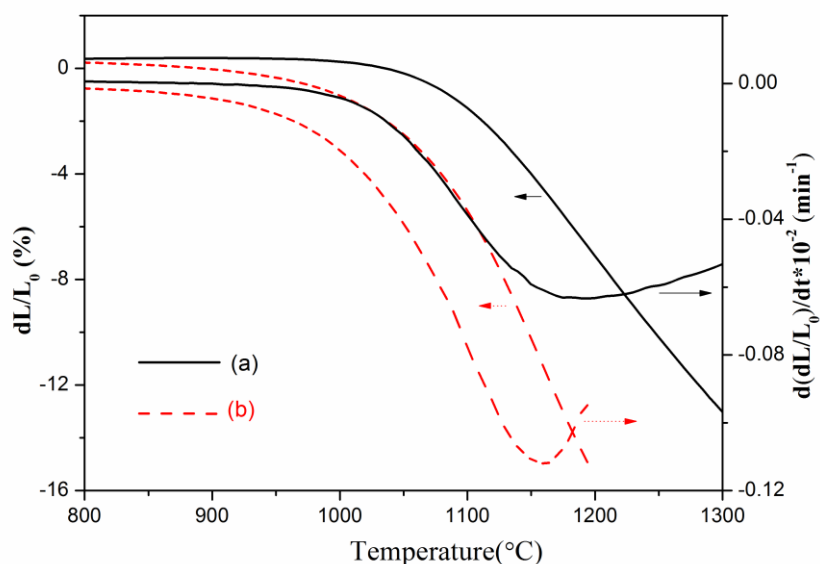


Figure 2. Dilatometric curves of (a) YSZ and (b) 3ZYSZ measured at a heating rate of 10°C/min in air.

Fig.3 shows the relative densities of YSZ and ZnO added YSZ sintered at 1150°C and 1200°C . In total, ZnO addition can effectively improve the relative densities, especially at 1150°C . At 1200°C , the relative densities of 2ZYSZ and 3ZYSZ are higher than 94%, which is high enough for the application as SOFC electrolyte. On the contrary, the relative density of YSZ sintered at 1200°C is only 82%.

The SEM images of the cross-section of YSZ, 2ZYSZ and 3ZYSZ sintered at 1200°C are given in Fig.4. Interconnected pores and spherical particles can be seen from Fig. 4a which means YSZ is in the intermediate stage of sintering. Isolated pores and clear grain boundary are observed for 2ZYSZ and 3ZYSZ which means they are in the final stage of sintering [13]. From the sintering behavior and microstructure, we can see that the sintering activity of YSZ was greatly improved by the addition of ZnO.

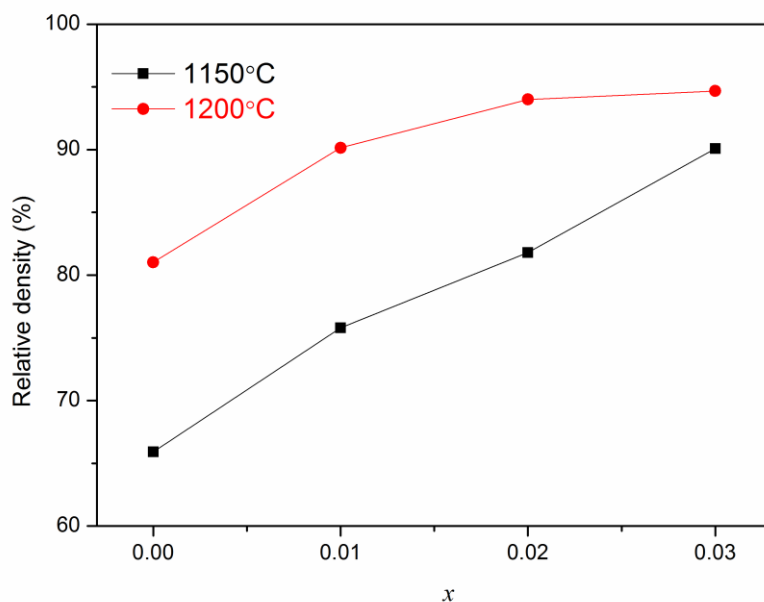
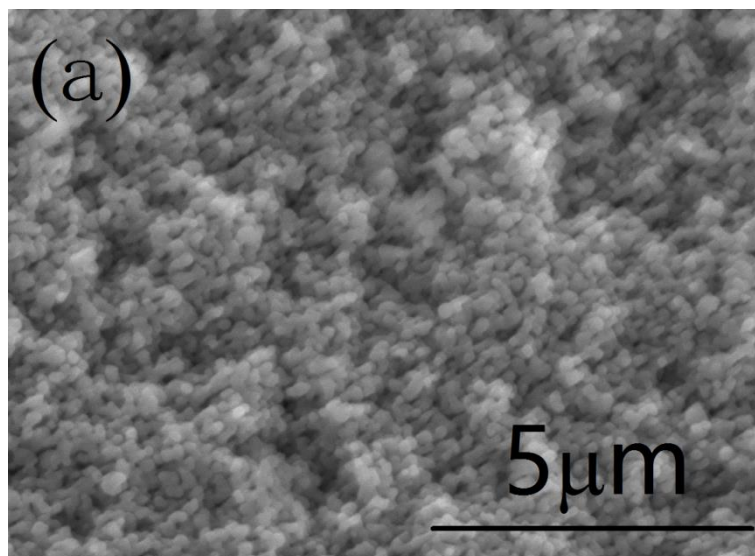


Figure 3. The relative densities of YSZ with and without ZnO addition sintered at 1150 and 1200 °C.

From Fig. 5 we can see that Zn mainly distributed at the grain boundary. Previous research showed that the transition metal oxides, such as CuO, Fe₂O₃, Mn₂O₃, et al, prefer to form the glass films at the grain boundary of the fluorite structure [14-16]. The rapid densification for the Zn-doped samples at relative lower sintering temperatures can be attributed to the formation of Zn-rich liquid phase films at the grain boundaries. In the presence of a liquid phase, particle rearrangement became easier and mass transport by grain-boundary diffusion took place much faster, leading to enhanced densification kinetics [14-17]. It can't be denied that some closed pores are still exist in Fig. 4b and 4c. From the preparation process, we know that the organic binder was used for the preparation of the green compacts.



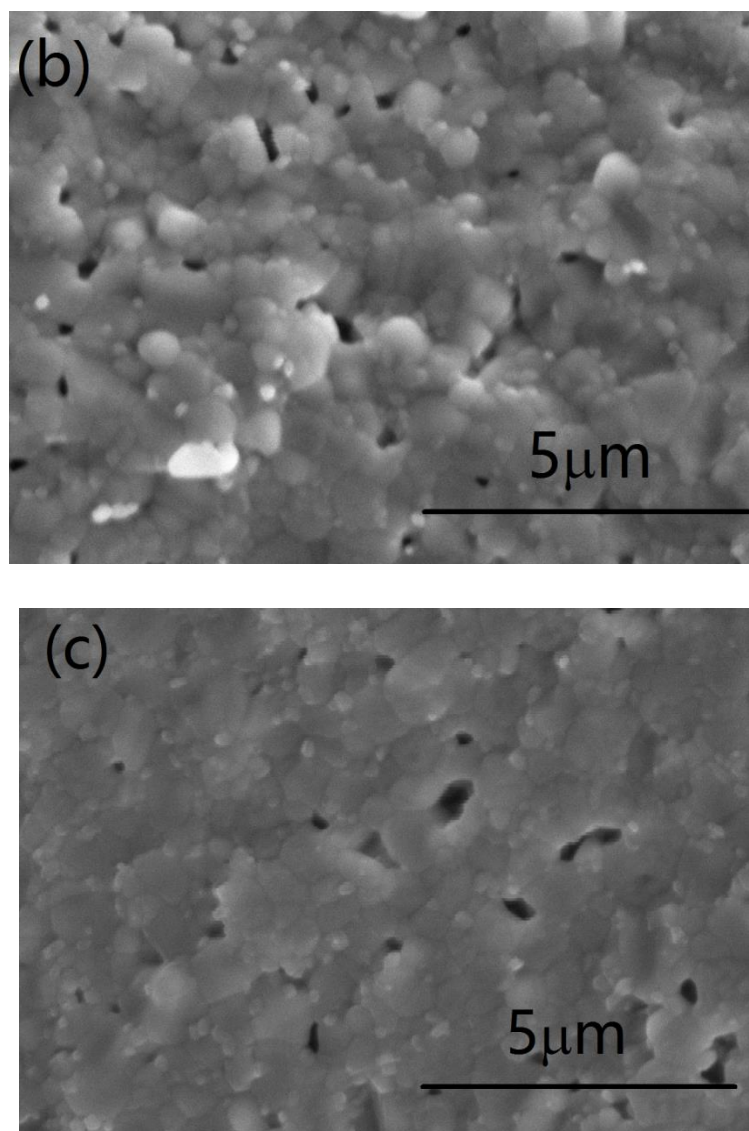


Figure 4. The cross-section SEM images of (a)YSZ, (b) 2ZYSZ, and (c) 3ZYSZ sintered at 1200 °C.

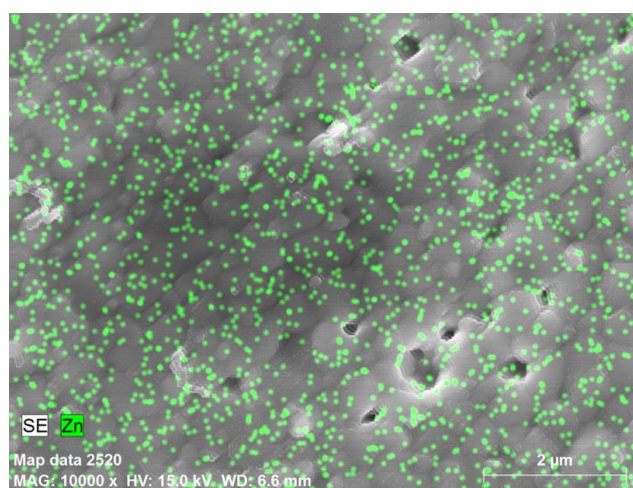


Figure 5. Zn elemental distribution in 1ZYSZ by EDX measurement.

Theoretically, pores can be removed effectively. But the binder burnout is a complex process involving the polymer decomposition, transport and diffusion of decomposed products, and removal of them. A number of parameters: ceramic body compact size, shrinkage rate, heating rate, organic polymer content affect burnout process. In fact, it is very difficult to remove the pores completely. [18]

The contributions of grain and grain boundary resistivity to the total ceramic resistance were estimated using impedance spectroscopy. Fig. 6 gives the results of YSZ, 1ZYSZ, 2ZYSZ, and 3ZYSZ sintered at 1200 °C measured at 700 °C. One semicircle is observed for each impedance curve. The high frequency intercept (the left intercept of the semicircle) with the real axis represents the grain interior resistivity, the low frequency intercept (the right intercept of the semicircle) corresponds to the total resistivity, and the difference between the high frequency and low frequency intercepts represents the apparent grain boundary resistivity [16]. The shape of the impedance spectra measured from 550 to 800 °C for each component are the same. The grain, grain boundary, and total resistivity can be extracted from the AC impedance spectra. And the conductivities can be calculated. Fig. 7 gives the apparent grain boundary, grain, and total conductivities of YSZ with different ZnO content measured from 550 to 800 °C. The grain boundary conductivity at 800 °C decreased from 0.077 to 0.044 S·cm⁻¹ with x increasing from 0 to 3. The grain and total conductivities first increased with ZnO content, then decreased with further increase in ZnO content. Compared with YSZ, the total conductivity of 2ZYSZ increased from 0.013 to 0.021 S·cm⁻¹. All grain, grain boundary, and total conductivities are in accordance with the Arrhenius relationship, as shown in Fig. 8. The activation energies can be calculate, as shown in table 1. Compared with YSZ, ZnO modified YSZ have higher activation energy. From Fig.5 we know that ZnO exists mainly at the grain boundary region. With the increase of ZnO addition, the layer of ZnO film increased. The insulation of ZnO leads to the increase of grain boundary conductivity with the increase of ZnO. Under low ZnO content, the grain conductivity is mainly affected by the relative density. The denser the electrolyte is, fewer pores will exist. For the ceramics with poor densification, the pores at the grain or grain boundary weaken the conductive channel, and the migration of oxygen ions is blocked by the pores. ZnO addition caused the increase of densification which led to the obvious increase of grain conductivity. But with further increase in ZnO addition, the ZnO second phase can also lead to the decrease of grain conductivity.

Table 1. The activation energies (E_a) of YSZ and ZnO modified YSZ

	E_a (eV)		
	grain boundary	grain	total
$x=0$	0.92	1.04	1.03
$x=0.01$	1.11	1.12	1.12
$x=0.02$	1.07	1.07	1.07
$x=0.03$	1.15	1.11	1.12

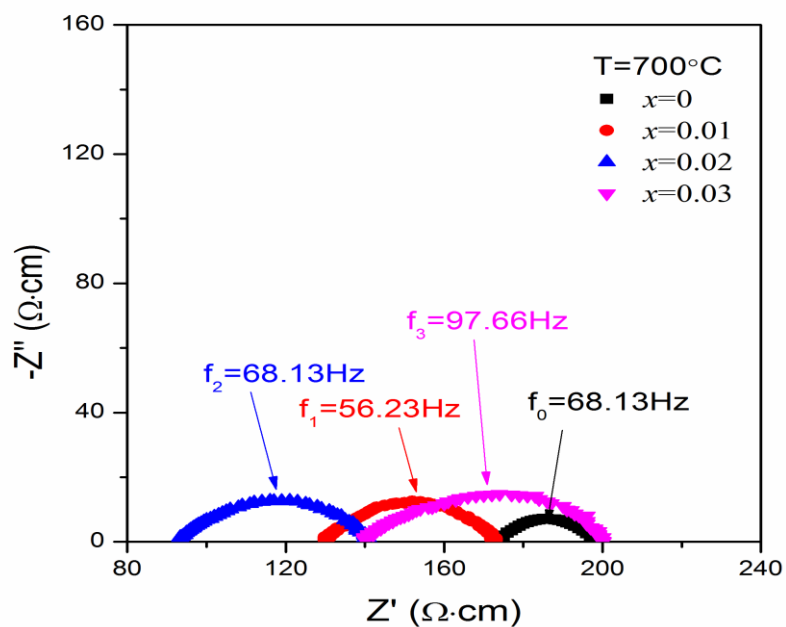
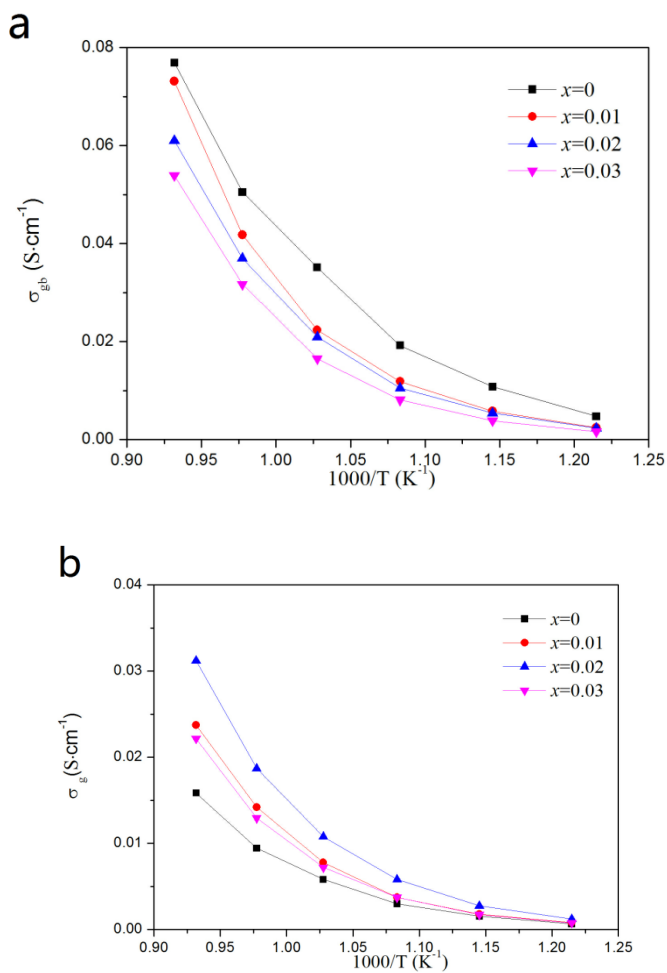


Figure 6. Impedance spectra of YSZ, 1YSZ, 2ZYSZ and 3ZYSZ sintered at 1200 °C measured at 700 °C.



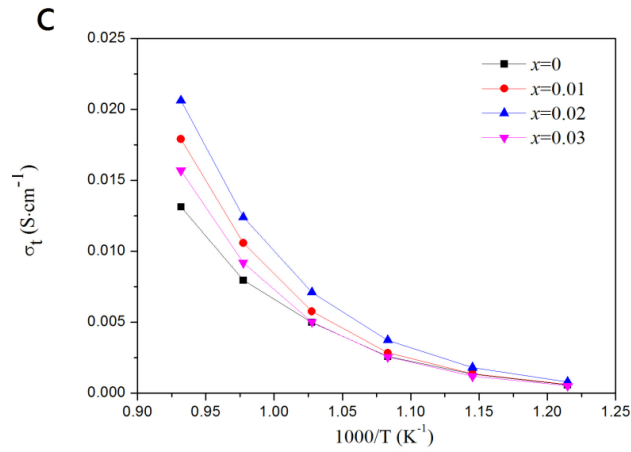
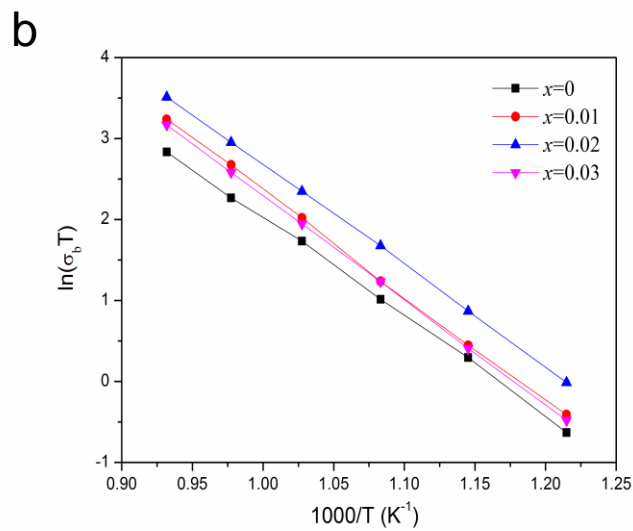
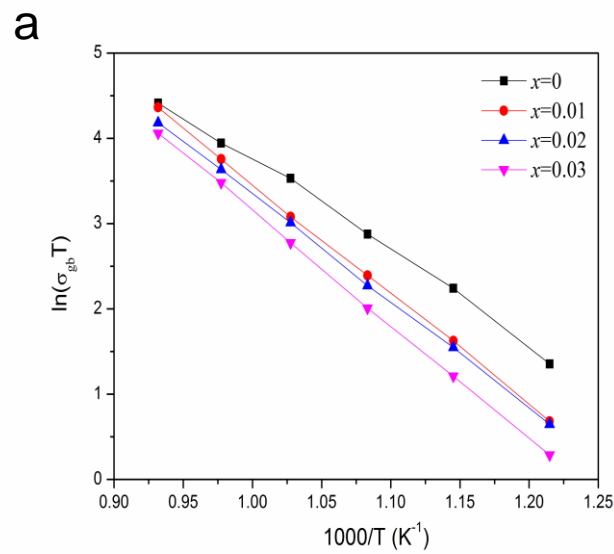


Figure 7. Apparent (a) grain boundary, (b) grain, and (c) total conductivities of YSZ with different ZnO content sintered at 1200 °C measured from 550 to 800 °C.



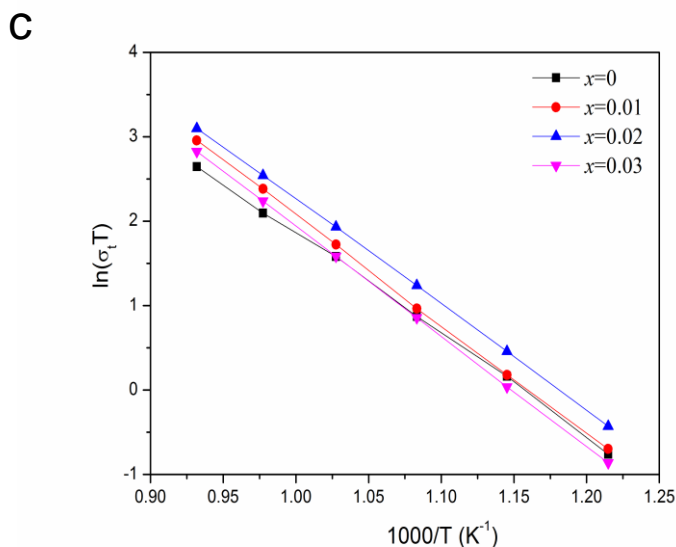


Figure 8. Relationship between $\ln(\sigma T)$ and the reciprocal of the absolute temperature ($1000/T$): (a) apparent grain boundary, (b) grain, and (c) total.

4. CONCLUSIONS

ZnO modified YSZ can achieve a relative density of 94% at 1200 °C. ZnO existed mainly as the glass film at the grain boundary. ZnO addition can lead to the decrease of grain boundary conductivity. But the grain and total conductivities increased with appropriate ZnO addition. The total conductivity of 2 mol% Zn modified YSZ is $0.021 \text{ S}\cdot\text{cm}^{-1}$. ZnO is an ideal sintering additive of YSZ which can effectively decrease the sintering temperature to 1200 °C.

ACKNOWLEDGEMENTS

This work is supported by National Natural Science Foundation of China (Grant no. 51102094), Shanghai Leading Academic Discipline Project (Grant no. B502), Shanghai Key Laboratory Project (Grant no. 08DZ2230500).

References

1. B. C. H. Steele, *J. Nature.*, 400 (1999) 619.
2. T. Baquero, J. Escobar, J. Frade, D. Hotza, *J. Ceram. Int.*, 39 (2013) 8279.
3. J. W. Fergus, *J. Power Sources.*, 162 (2006) 30.
4. S. Hao, C. Wang, T. Liu, J. Wang, Z. Mao, *J. Ceram. Int.*, 42 (2016) 9323.
5. C. Zhao, R. Liu, S. Wang, T. Wen, *J. Electrochem. Commun.*, 11(2009) 842.
6. H. Yao, X. Wang, R. Pei, J. Wang, Z. Li, *J. Ceram. Int.*, 37 (2011) 3153.
7. H. Zhao, X. Li, F. Ju, U. Pal, *J. Mater. Process. Technol.*, 200 (2008) 199.
8. R. F. Marcomini, D. P. F. Souza, M. Kleitz, L. Dessemond, M. C. Steil, *J. solid State Sci. Technol.*, 1 (2012) N127.
9. S. Nakayama, *J. Mater. Sci.*, 41 (2006) 1631.

10. Y. Liu, L. E. Lao, *J. Solid State Ionics.*, 177 (2006) 159.
11. J. Kimpton, T.H. Randle, *J. Solid State Ionics.*, 149 (2002) 89.
12. J. A. Dean, *Lange's Handbook of Chemistry, 15th ed.*, McGraw-Hill, INC., New York, 1999.
13. M. N., Rahaman, *Ceramic Processing and Sintering, 2nd ed.*, CRC Press, Boca Raton, 2003.
14. Q. Lv, X. Dong, Z. Zhu, Y. Dong, *J. Ceram. Int.*, 40 (2014) 11545.
15. D. P. Fagg, J. C. C. Abrantes, D. Pérez-Coll, P. Núñez, V. V. Kharton, J. R. Frade, *J. Electrochim. Acta.*, 48 (2003) 1023.
16. H. Yao, X. Zhao, X. Chen, J. Wang, Q. Ge, J. Wang, Z. Li, *J. Power Sources.*, 205 (2012) 180.
17. C. Tseng, P. Chen, P. Lin, *J. Alloys Compd.*, 632 (2015) 810.
18. T. Ertugrul, S. Celik, M. Mat, *J. Power Sources.*, 242(2013) 775.

© 2017 The Authors. Published by ESG (www.electrochemsci.org). This article is an open access article distributed under the terms and conditions of the Creative Commons Attribution license (<http://creativecommons.org/licenses/by/4.0/>).